Growth of hexagonal boron nitride on (111) Si for deep UV photonics and thermal neutron detection

K. Ahmed, R. Dahal, A. Weltz, J.-Q. Lu, Y. Danon, and I. B. Bhat

Citation: Applied Physics Letters **109**, 113501 (2016); doi: 10.1063/1.4962831
View online: http://dx.doi.org/10.1063/1.4962831
View Table of Contents: http://scitation.aip.org/content/aip/journal/apl/109/11?ver=pdfcov
Published by the AIP Publishing

Articles you may be interested in

Growth and device processing of hexagonal boron nitride epilayers for thermal neutron and deep ultraviolet detectors
AIP Advances **6**, 075213 (2016); 10.1063/1.4959595

Direct growth of nanocrystalline hexagonal boron nitride films on dielectric substrates
Appl. Phys. Lett. **106**, 101901 (2015); 10.1063/1.4914474

High quality single atomic layer deposition of hexagonal boron nitride on single crystalline Rh(111) four-inch wafers
Rev. Sci. Instrum. **85**, 035101 (2014); 10.1063/1.4866648

Dielectric strength, optical absorption, and deep ultraviolet detectors of hexagonal boron nitride epilayers
Appl. Phys. Lett. **101**, 171112 (2012); 10.1063/1.4764533

APL Photonics

NEW Special Topic Sections
NOW ONLINE
Lithium Niobate Properties and Applications: Reviews of Emerging Trends
AIP Applied Physics Reviews

Reuse of AIP Publishing content is subject to the terms at: https://publishing.aip.org/authors/rights-and-permissions. Download to IP: 128.113.44.9 On: Wed, 23 Nov 2016 18:21:49

APPLIED PHYSICS LETTERS **109**, 113501 (2016)

Growth of hexagonal boron nitride on (111) Si for deep UV photonics and thermal neutron detection

K. Ahmed,[1,a)] R. Dahal,[1] A. Weltz,[2] J.-Q. Lu,[1] Y. Danon,[2] and I. B. Bhat[1,b)]
[1]*Department of Electrical, Computer, and Systems Engineering, Rensselaer Polytechnic Institute, Troy, New York 12180, USA*
[2]*Department of Mechanical, Aerospace and Nuclear Engineering, Rensselaer Polytechnic Institute, Troy, New York 12180, USA*

(Received 23 June 2016; accepted 2 September 2016; published online 15 September 2016)

Hexagonal boron nitride (hBN) growth was carried out on (111) Si substrates at a temperature of 1350 °C using a cold wall chemical vapor deposition system. The hBN phase of the deposited films was identified by the characteristic Raman peak at 1370 cm^{-1} with a full width at half maximum of 25 cm^{-1}, corresponding to the in-plane stretch of B and N atoms. Chemical bonding states and composition of the hBN films were analyzed by X-ray photoelectron spectroscopy; the extracted B/N ratio was 1.03:1, which is 1:1 within the experimental error. The fabricated metal-hBN-metal devices demonstrate a strong deep UV (DUV) response. Further, the hBN growth on the vertical (111) surfaces of parallel trenches fabricated in (110) Si was explored to achieve a thermal neutron detector. These results demonstrate that hBN-based detectors represent a promising approach towards the development of DUV photodetectors and efficient solid-state thermal neutron detectors. *Published by AIP Publishing.* [http://dx.doi.org/10.1063/1.4962831]

Hexagonal boron nitride (hBN) is a layered compound semiconductor with a crystalline structure and a number of properties parallel to those of graphene, including a low dielectric constant, high temperature stability, and piezoelectricity.[1–3] hBN is an emerging deep UV (DUV) photonics material,[1–3] since it has a large bandgap with reported values of 5.6–6 eV.[4–7] Since ^{10}B is one of the constituent elements in hBN with a large thermal neutron absorption cross-section (3840 barns),[8] solid-state neutron detector (SSND) fabrication using hBN is a recent application of interest.[9] Other SSNDs are fabricated using the Si p-n junction coated with either ^{10}B or ^{7}Li and these are heterogeneous as their neutron converting and charge collecting regions are different.[8,10,11] hBN SSNDs are homogeneous detectors because hBN is utilized as both the neutron converter and charge-collector medium, potentially allowing for higher intrinsic thermal neutron detection efficiencies. When an incident neutron is absorbed by a ^{10}B atom in hBN, energetic alpha particles and ^{7}Li ions are produced. Full energy deposition of these energetic particles in hBN is possible and can produce a large number of electron-hole-pairs (EHPs), which, when collected, lead to a detectable pulse indicating a neutron event. Additionally, the low atomic numbers of B and N (5 and 7, respectively) mean hBN SSNDs will have a low gamma sensitivity, which is an important characteristic of a good neutron detector. This paper reports on high temperature (1350 °C) growth of hBN on planar (111) Si substrates and (111) Si vertical surfaces by chemical vapor deposition (CVD) for the fabrication of DUV photodetectors and thermal neutron detectors. hBN growth on Si is highly attractive because of the prospect of a large-scale and low-cost mass production of hBN-based devices. Design, fabrication, and characterization of hBN devices of two different configurations were performed, with charge collection along the highest electron mobility path in hBN, i.e., a-axis of hBN.[12] The first configuration is a planar metal-semiconductor-metal (MSM) structure. The second one is a hBN-Si template detector which involves hBN growth on (111) Si vertical facets of parallel trenches etched in a (110) oriented Si substrate. Our simulation indicates that the theoretical requirement of hBN thickness (assuming 100% ^{10}B) is 35 μm for a neutron detection efficiency of 50% and 80 μm for an efficiency of 80%. Growing such thick, highly crystalline hBN films on the Si substrate is challenging. hBN-Si template detectors can circumvent this challenge, since the thickness of hBN grown on trench sidewalls is determined by the half-width of the trench (i.e., a few microns) and neutron interaction length is equal to the trench depth (i.e., tens of microns). For hBN-Si template detectors, Si is not used as a semiconductor material but rather as a conductor and as a support wafer. hBN MSM and hBN-Si template devices both show strong response to DUV light. hBN-Si template devices also respond to thermal neutrons. These are the first demonstrations of such detection capabilities for hBN grown on Si.

In-plane lattice constants of hBN and (111) Si are 2.5 Å and 3.83 Å,[13,14] respectively, implying a lattice mismatch of 34.7%, which represents a significant challenge associated with the direct epitaxial growth of hBN on (111) Si. Very few attempts have been reported on the hBN growth on Si. Previous reports of CVD growth of hBN on (111) Si used single source precursors (e.g., borane–triethylamine complex and polyborazylene) and growth temperatures $\leq$1000 °C.[15,16] Those films were found to be turbostratic hBN or nanocrystalline hBN, a less ordered form of hBN. Separate precursor gases were used for B (triethylboron, TEB) and N (ammonia, NH_3) for hBN growth on (111) Si in this work. The growth temperature (T_G) is limited by the melting point of Si

a)Electronic mail: ahmedk2@rpi.edu
b)Electronic mail: bhati@rpi.edu

Reuse of AIP Publishing content is subject to the terms at: https://publishing.aip.org/authors/rights-and-permissions. Download to IP: 128.113.44.9 On: Wed, 23 Nov 2016 18:21:49

(1414 °C) and the maximum employed T_G was 1350 °C. Further, NH_3 reacts with Si at the growth temperatures, forming amorphous silicon nitride that may inhibit subsequent epitaxial hBN growth. An optimized pre-deposition of a few layer of B on the Si substrate before introducing NH_3 into the reactor is therefore a necessary step. For epitaxial growth of AlN on (111) Si with trimethylaluminium (TMAl) and NH_3 precursors, some groups have used an Al pre-deposition step using TMAl before AlN growth.[17–19] The knowledge of high temperature CVD growth of AlN on (111) Si has been adopted for CVD growth of hBN on (111) Si in this work.

hBN growth on (111) Si wafers was carried out in a horizontal cold wall, low pressure CVD system. Silicon carbide (SiC)-coated graphite susceptors were used to heat the substrates utilizing an induction heating system. (111) Si substrates were dipped in a 2% hydrofluoric acid solution for 2 min to remove the native oxide from the surface and get the surface hydrogen terminated. The substrates were exposed to TEB (with a flow rate of 0.5 μmol/s) for B pre-deposition for 20 s at a temperature of 1350 °C. hBN growth was then initiated by introducing NH_3 to the reactive gas mixture at the same temperature. The flow rates of TEB and NH_3 were kept fixed at 0.5 μmol/s and 150 μmol/s, respectively, implying a V/III ratio of 300. The chamber pressure was 100 Torr, and the growth atmosphere was H_2 with a flow of ~2000 sccm. hBN growth was also performed on the (111) Si vertical trench sidewalls (etched in (110) Si) using the CVD system with the same surface preparation and growth recipe as the hBN growth on planar (111) Si substrates.

Raman spectroscopy was used to investigate the bonding characteristics, phonon features, and phase purity of the films. hBN has a characteristic Raman scattering peak at 1366 cm^{-1}, which corresponds to the in-plane E_{2g} phonon mode of hBN.[1,20] For this doubly degenerate optical phonon mode, the B and N atoms in each plane move in the opposite directions. The contributions from the two planes cancel each other and this mode does not have an LO-TO splitting. Raman spectra for the grown films were collected using a Witec Alpha 300 R confocal Raman imaging system with a 532 nm laser excitation source. The films showed Raman peaks at 1370 cm^{-1} with a FWHM of 25 cm^{-1}, which confirms the successful growth of hBN. Figure 1(a) shows the Raman spectrum of a representative 1.6 μm thick hBN film.

Broadening and shifting of Raman modes in nanocrystalline materials were explained in Ref. 21 through the relaxation of the usual q = 0 momentum selection rule. Nemanich *et al.* extended this model for hBN.[22] As the crystallite size is reduced to nanoscale, the uncertainty of the phonon wave vector participating in the first order Raman scattering becomes $\approx 2\pi/L_a$, where L_a is the size of the crystallites.[22] For most crystalline solids, a red shift (i.e., decrease in frequency) and broadening of the Raman peak are expected with smaller L_a, since optical phonon frequency (ω) decreases with increasing q from a maximum value at q = 0 (i.e., Brillouin zone center). But for smaller L_a, hBN films show a blue shift (i.e., increase in frequency) and broadening of the Raman active mode, since hBN has an unusual dispersion curve where ω is not maximum at q = 0 and increases with increasing q values.[22] For the grown hBN films, a Raman peak with a blue shift of 4 cm^{-1} and a FWHM of 25 cm^{-1} indicates the films to be turbostratic hBN or nanocrystalline hBN. Similar upshifted Raman scattering spectra with larger FWHM values were seen in nanocrystalline hBN films grown on sapphire by other groups.[23,24] L_a of the hBN films can be calculated using $\Gamma_{1/2} = 141.7(L_a)^{-1} + 8.7$, where L_a is in nm and $\Gamma_{1/2}$ is the FWHM of the Raman peak in cm^{-1}.[22] The crystallite size was estimated as ~9 nm for the hBN films grown on (111) Si at 1350 °C.

The influence of T_G on the hBN film quality was investigated. Three films were grown at different temperatures, each for the duration of 1 h. Figure 1(b) shows the Raman spectra of these films. As T_G decreases from 1350 °C to 1230 °C, the Raman peak becomes weaker and broader, meaning that the crystallite size becomes smaller with lower T_G values. T_G = 1100 °C does not favor hBN growth as evident by the absence of the Raman peak for the corresponding film.

Elemental composition of the hBN films was analyzed using a Phi Versaprobe X-Ray Photo-Electron Spectroscopy (XPS) system with a focused monochromatic Al Kα x-ray source (with an energy of 1486.6 eV). Figures 2(a) and 2(b) show the B 1 s and N 1 s XPS peaks for the B-N bonding state (of the same 1.6 μm thick hBN film) at the binding energies of 190.7 eV and 398.3 eV, respectively, which are in good agreement with the reported values in the literature.[5,25,26] A single dominant and highly symmetric XPS peak was observed for each of the B 1 s and N 1 s spectra, indicating the presence of only sp^2-hybridized B and N atoms in the film. The estimated B/N ratio is 1.03:1, indicating 1:1 stoichiometry within the XPS experimental error. Furthermore, excellent sample uniformity is found in the film suggested by the similar atomic compositions across the sample.

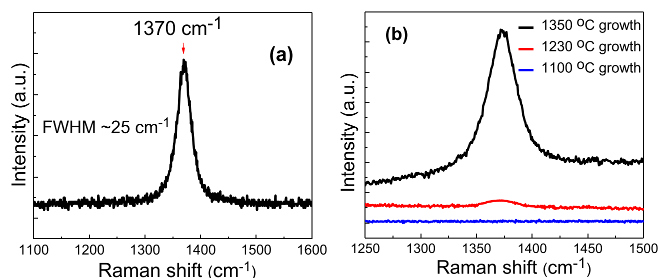

FIG. 1. (a) The Raman spectrum of a 1.6 μm thick hBN film grown at 1350 °C and (b) Raman spectra of the films grown at different temperatures.

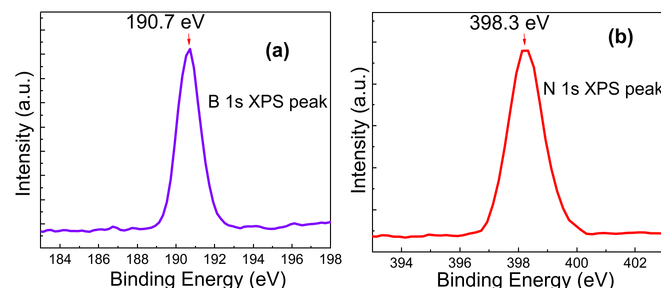

FIG. 2. (a) B 1 s and (b) N 1 s XPS spectra of a 1.6 μm thick hBN film.

Reuse of AIP Publishing content is subject to the terms at: https://publishing.aip.org/authors/rights-and-permissions. Download to IP: 128.113.44.9 On: Wed, 23 Nov 2016 18:21:49

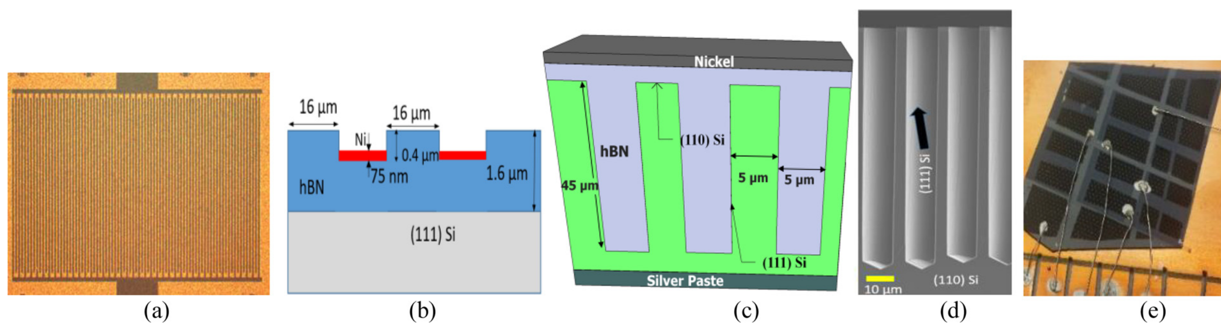

FIG. 3. (a) The optical microscopy image and (b) the schematic of a $3 \times 2\,\mathrm{mm}^2$ area MSM device. (c) The schematic of an hBN-Si template detector. The actual detector has an area of $0.36\,\mathrm{cm}^2$. (d) A cross-sectional scanning electron microscopy (SEM) image of a typical Si template used for hBN growth. (e) The optical image of an array of hBN-Si template devices with different areas.

MSM devices were fabricated using the hBN films. Figures 3(a) and 3(b) show the optical microscopy image and the schematic, respectively, of an MSM device fabricated using a 1.6 μm thick hBN film. The width of the inter-digital fingers is 16 μm, and the spacing between the fingers is 16 μm. The device has an area of $3 \times 2\,\mathrm{mm}^2$. Etching of hBN was performed with an inductively coupled plasma-reactive ion etching (ICP-RIE) process using SF_6 plasma. Inter-digital fingers were realized by 75 nm Ni (e-beam evaporated). Figure 3(c) shows the schematic of a device fabricated with hBN filled parallel trenches in lightly doped n-type (110) Si, where hBN was grown on the vertical (111) Si trench sidewalls. Trench sidewalls were etched in (110) Si using tetramethylammonium hydroxide (TMAH). The trenches are separated by 5 μm thick Si walls and have a width of 5 μm and a depth of $\sim$45 μm. Front and back contacts were 10 nm Ni (e-beam evaporated) and silver paste, respectively. The energetic alpha particles (from the absorption of neutron in hBN) have a range of $\sim$5 μm in Si, while ^{7}Li ions have an even lower range in Si.[8] Hence, these particles can produce EHPs in the 5 μm wide Si walls and the Si below the trench bottoms with a depth (d) of 5 μm from the trench bottoms. But these EHPs cannot be separated without the presence of the electric field there, since the trench walls and the region below the trench bottoms (with $d \gg 5\,\mu$m) became highly p-type (i.e., equipotential) during the hBN growth process at 1350 °C for $\sim$7 h, as demonstrated by theoretical calculations. The diffusion length of the electrons in this region is also expected to be smaller than the junction depth, if any. It verifies the role of Si as a conductor and a supporting wafer for the hBN-Si template device.

The $3 \times 2\,\mathrm{mm}^2$ area MSM device (shown in Fig. 3(b)) and a representative $0.36\,\mathrm{cm}^2$ area hBN-Si template device (shown in Fig. 3(c)) were tested for DUV excitation response using a UVP pen ray lamp. This lamp has an intensity of 160 μW/cm^2 at a distance of 0.75 in. (corresponding to the DUV wavelength of 184.9 nm). Both devices demonstrated strong DUV response, which can be seen in the corresponding I–V measurement data in Figs. 4(a) and 4(c). No noticeable persistent photoconductivity (PPC) was observed for the devices, as suggested by the photocurrent decay kinetics of the MSM device (for a bias voltage of 95 V) shown in Fig. 4(b) and the hBN-Si template device (for a bias voltage of 180 V) shown in Fig. 4(d). For both devices, current remains the same when room light is turned on from the dark state or when exposed to strong visible light. For the MSM device, it implicates that the current path does not involve Si and is only through hBN strips between the electrodes. A current path through Si would have resulted in a much higher current under room light compared to dark current.

The same $0.36\,\mathrm{cm}^2$ area hBN-Si template detector was tested with a 1.0 kBq ^{241}Am alpha source (with 5.5 MeV energy) and a ^{252}Cf neutron source. Pulse height spectra were collected using an ORTEC 142PC preamplifier, an ORTEC 672 spectroscopy amplifier, and an ORTEC ASPEC-927 multichannel analyzer (MCA). The alpha response was measured by placing the ^{241}Am alpha source on top of the device biased with 400 V. Figure 5(a) shows the pulse height spectra for the detector with and without the presence of the alpha source, demonstrating the detection of alpha irradiation. The neutron response of the same device was measured by exposing it to a ^{252}Cf neutron source moderated by a high-density polyethylene (HDPE) housing. A 100-min exposure of the device to the neutron source with a bias of 400 V gave rise to a pulse height spectrum shown in Fig. 5(b), clearly indicating the device's response to neutrons.

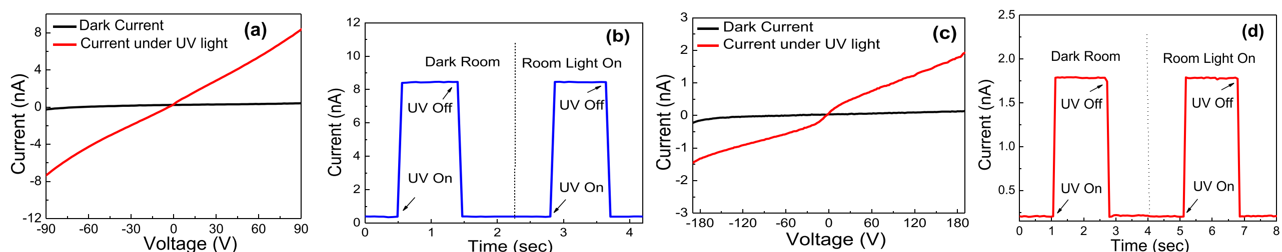

FIG. 4. (a) The I–V characteristics and (b) the photocurrent decay kinetics (with 95 V applied voltage) of the $3 \times 2\,\mathrm{mm}^2$ area MSM device (shown in Fig. 3(b)). (c) The I–V characteristics and (b) the photocurrent decay kinetics (with 180 V applied voltage) of the $0.36\,\mathrm{cm}^2$ area hBN-Si template device (shown in Fig. 3(c)).

Reuse of AIP Publishing content is subject to the terms at: https://publishing.aip.org/authors/rights-and-permissions. Download to IP: 128.113.44.9 On: Wed, 23 Nov 2016 18:21:49

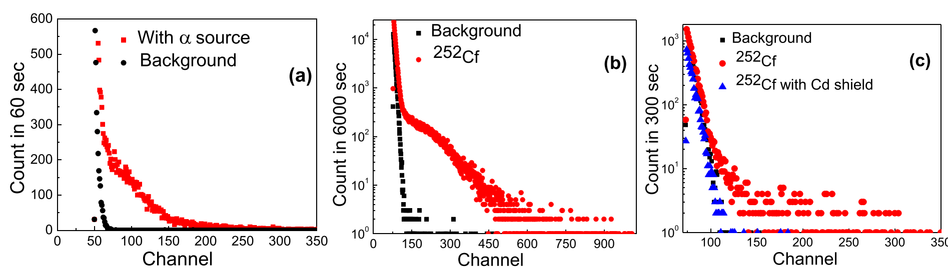

FIG. 5. Pulse height distribution of (a) alpha irradiation and (b) thermal neutrons measured with the hBN-Si template detector shown in Fig. 3(c). (c) Pulse height distribution of the same detector for intrinsic thermal neutron detection efficiency calculation.

In order to measure intrinsic thermal neutron detection efficiency of the hBN-Si template detector, three separate measurements were performed, each with a bias voltage of 400 V for 300 s with the detector placed 8 cm away from the ^{252}Cf moderator face. Thermal neutron flux of 320 n/cm^2 s was measured at this position by the gold foil activation method. One measurement was with the bare device and another one was with the device covered by Cd. The moderated ^{252}Cf source emits fast neutrons and gamma rays in addition to thermal neutrons. Since Cd blocks fast neutrons and gamma rays, the difference in the count (C_{Bare}-C_{Cd}) is caused by thermal neutrons. The third measurement was taken with ^{252}Cf away from the moderator housing to obtain the electronic noise level. The detection efficiency was measured to be $1.1 \pm 0.2\%$ for the 0.36 cm^2 area device. hBN growth in this work was done with natural TEB due to the easy availability of TEB with natural boron (19.9% ^{10}B). The efficiency can be a factor of 5 higher if TEB with enriched boron (∼100% ^{10}B) was used. Detection efficiency for these devices can be enhanced further by improving the crystalline quality of hBN grown on (111) Si trench sidewalls and by the optimization of the device structure and fabrication processes. The hBN-Si template device represents the first reported DUV and thermal neutron detector using hBN films grown on Si.

In summary, hBN films were grown on (111) Si substrates using a cold wall CVD system. A Raman peak at 1370 cm^{-1} confirms the hBN phase, while the blue shift and spectral width of the peak indicate the films to be nanocrystalline. XPS analysis confirmed the stoichiometric hBN phase and excellent uniformity of the films. Planar MSM devices were fabricated using hBN grown on (111) Si substrates. hBN-Si template detectors were fabricated with hBN growth on the vertical (111) Si facets of the parallel trenches. Both device configurations work as DUV photodetectors as evidenced from their strong response to DUV excitation. Pulse height spectra measurements demonstrate the alpha and neutron detection capability of the hBN-Si template detectors. The development of practical and functional SSNDs with each configuration is anticipated with further improvement in the crystalline quality of hBN grown on planar (111) Si and vertical (111) Si facets of trenches. Additionally, using enriched TEB precursors, improvements in the device design, and maturation of the fabrication techniques should improve the performance of these hBN-based SSNDs.

The authors are grateful to the staff of the Rensselaer Polytechnic Institute Micro and Nano Fabrication Clean Room (RPI MNCR) for their support. This work was supported by the U.S. Department of Homeland Security, Domestic Nuclear Detection Office, under the Grant Nos. ECCS-1348269 and 2013-DN-077-ER001.

[1]M. Chubarov, H. Pedersen, H. Högberg, V. Darakchieva, J. Jensen, P. Persson, and A. Henry, Phys. Status Solidi RRL **5**, 397 (2011).
[2]K. Watanabe, T. Taniguchi, T. Niiyama, K. Miya, and M. Taniguchi, Nat. Photonics **3**, 591 (2009).
[3]R. Dahal, J. Li, S. Majety, B. N. Pantha, X. K. Cao, J. Y. Lin, and H. X. Jiang, Appl. Phys. Lett. **98**, 211110 (2011).
[4]Y. Kubota, K. Watanabe, O. Tsuda, and T. Taniguchi, Science **317**, 932 (2007).
[5]R. Y. Tay, S. H. Tsang, M. Loeblein, W. L. Chow, G. C. Loh, J. W. Toh, S. L. Ang, and E. H. T. Teo, Appl. Phys. Lett. **106**, 101901 (2015).
[6]G. Cassabois, P. Valvin, and B. Gil, Nat. Photonics **10**, 262 (2016).
[7]J. H. Edgar, T. B. Hoffman, B. Clubine, M. Currie, X. Z. Du, J. Y. Lin, and H. X. Jiang, J. Cryst. Growth **403**, 110 (2014).
[8]R. Dahal, K. C. Huang, J. Clinton, N. LiCausi, J.-Q. Lu, Y. Danon, and I. Bhat, Appl. Phys. Lett. **100**, 243507 (2012).
[9]T. C. Doan, S. Majety, S. Grenadier, J. Li, J. Y. Lin, and H. X. Jiang, Nucl. Instrum. Methods Phys. Res., Sect. A **783**, 121 (2015).
[10]D. S. McGregor, W. J. McNeil, S. L. Bellinger, T. C. Unruh, and J. K. Shultis, Nucl. Instrum. Methods Phys. Res., Sect. A **608**, 125 (2009).
[11]R. J. Nikolic, A. M. Conway, C. E. Reinhardt, R. T. Graff, T. F. Wang, N. Deo, and C. L. Cheung, Appl. Phys. Lett. **93**, 133502 (2008).
[12]R. Dahal, K. Ahmed, J. W. Wu, A. Weltz, J.-Q. Lu, Y. Danon, and I. Bhat, Appl. Phys. Express **9**, 065801 (2016).
[13]T. Löher, K. Ueno, and A. Koma, Appl. Surf. Sci. **130–132**, 334 (1998).
[14]W. Paszkowicz, J. B. Pelka, M. Knapp, T. Szyszko, and S. Podsiadlo, Appl. Phys. A **75**, 431 (2002).
[15]C. Rohr, J.-H. Boo, and W. Ho, Thin Solid Films **322**, 9 (1998).
[16]M. S. Bresnehan, M. J. Hollander, M. Wetherington, K. Wang, T. Miyagi, G. Pastir, D. W. Snyder, J. J. Gengler, A. A. Voevodin, W. C. Mitchel, and J. A. Robison, J. Mater. Res. **29**, 459 (2014).
[17]X. Wang, H. Li, J. Wang, and L. Xiao, Electron. Mater. Lett. **10**, 1069 (2014).
[18]S. J. Bak, D.-H. Mun, K. C. Jung, J. H. Park, H. J. Bae, I. W. Lee, J.-S. Ha, T. Jeong, and T. S. Oh, Electron. Mater. Lett. **9**, 367 (2013).
[19]J. Cao, S. Lin, G. Fan, Y. Zhang, S. Zheng, Y. Yin, J. Huang, and J. Su, J. Cryst. Growth **312**, 2044 (2010).
[20]Y. Kobayashi and T. Akasaka, J. Cryst. Growth **310**, 5044 (2008).
[21]H. Richter, Z. P. Wang, and L. Ley, Solid State Commun. **39**, 625 (1981).
[22]R. J. Nemanich, S. A. Solin, and R. M. Martin, Phys. Rev. B **23**, 6348 (1981).
[23]M. Snure, Q. Paduano, M. Hamilton, J. Shoaf, and J. M. Mann, Thin Solid Films **571**, 51 (2014).
[24]Q. S. Paduano, M. Snure, J. Bondy, and T. W. C. Zens, Appl. Phys. Express **7**, 071004 (2014).
[25]L. Wang, B. Wu, L. Jiang, J. Chen, Y. Li, W. Guo, P. Hu, and Y. Liu, Adv. Mater. **27**, 4858 (2015).
[26]K. K. Kim, A. Hsu, X. T. Jia, S. M. Kim, Y. M. Shi, M. Hofmann, D. Nezich, F. Joaquin, M. Dresselhaus, T. Palacios, and J. Kong, Nano Lett. **12**, 161 (2012).

Reuse of AIP Publishing content is subject to the terms at: https://publishing.aip.org/authors/rights-and-permissions. Download to IP: 128.113.44.9 On: Wed, 23 Nov 2016 18:21:49